CHARACTERIZATION OF SHALES WITH LOW FIELD NMR

M. Fleury

IFP Energies nouvelles, 1 avenue de Bois-Préau, 92852 Rueil-Malmaison, France.

This paper was prepared for presentation at the International Symposium of the Society of Core Analysts held in Avignon, September 8th-11th,France

ABSTRACT

Nuclear Magnetic Resonance (NMR) relaxation methods are key techniques for evaluating shales, both from cores and logging data. First, very small pore sizes, down to nano-meter length scales, can be detected and quantified if the NMR tool has the ability to measure relaxation times in the range [0.1 – 1 ms], and second the different proton populations (water, oil, gas, organic matter) can be distinguished using 2D T_1-T_2 maps.
In this work, we show two techniques to characterize shales: 2D relaxation techniques to identify fluids, and deuterium tracer techniques to identify connectivity of the pore network system, providing also a measure of tortuosity. We used a NMR instrument working at a higher frequency (20 MHz) that yields a much higher sensitivity than standard plug-size benchtop apparatus. T_1-T_2 maps were acquired on different samples at different saturation states (dry, 100% water and 100% gas saturated). In such maps, the fluid typing is based on the T_1/T_2 ratio and T_2 values. One can detect different populations of protons: hydroxyls from the clay (T_2<0.1 ms, 10<T_1/T_2<100), water (T_1/T_2~2), and in certain situations organic matter (10< T_1/T_2<100). Methane can be clearly distinguished with T_1/T_2~10.

INTRODUCTION

The characterization of gas shales remains a challenge and cannot be performed using conventional petrophysical techniques. Even for basic properties such as porosity and permeability, appropriate protocols and instrumentation are required. For the visualisation of the pore space, we rely on recent microscopy techniques (Scanning Electronic Microscopy coupled with Focused Ion Beam) that are appropriate at nanometre scale. NMR relaxation techniques are also very appropriate in this context because it can detect small quantity of water or gas, in very small pore sizes. For example in the interlayer space of smectites, it is possible with an appropriate instrument to detect and quantify the water content even when the pore width is only one or two water layers thick [1]. However, for complex porous media such as shales, standard T_2 relaxation distributions provide limited information. There are many recent efforts to use advanced and/or multidimensional NMR techniques for separating the different proton contributions [2–

4]. As with conventional reservoirs, diffusion contrasts between gas, oil and water can be used to identify fluid phases. Another method is to use the T_1/T_2 contrast, and this is developed in this work.

We first recall the NMR relaxation theory for different proton populations and in the context of nano-porous media, for liquid, gas, and also for solids. The NMR instrument and the methane high pressure cell are then described. We studied organic matter extracted from different shales, and shales in different saturation states. We finally propose a T_1-T_2 fluid mapping based on our observations.

NMR THEORY

Relaxation of water in nanoporous media

For water in porous media, the dominant relaxation process is the result of interactions between the spins carried by molecules exploring the pore space by diffusion, and the electronic spins at the solid surface. These interactions are effective only close to the surface in a layer of thickness ε_S (<0.5 nm) and are characterized by a decay time constant T_S. Similarly, far from the surface, the intra and intermolecular interactions are characterized by a much longer decay time constant T_B. In a pore, let us define two regions: a bulk volume with a volume fraction f_b , and a surface layer with a volume fraction f_s ($f_b + f_s = 1$). Due to molecular diffusion, there is an exchange between the surface and bulk volumes with a typical exchange time τ_{ex}. In the so-called fast exchange regime ($\tau_{ex} << T$) or fast diffusion regime, the measured relaxation rate $1/T$ is an average of the bulk and surface relaxation rates weighted by the volume fraction:

$$\frac{1}{T_2} = \frac{f_s}{T_{2s}} + \frac{f_B}{T_{2B}} \approx \frac{S_p}{V_p}\frac{\varepsilon_S}{T_{2s}} + \frac{1}{T_{2B}} \qquad (1)$$

We show here the transverse relaxation time T_2 but the equation is also valid for the longitudinal relaxation with, however, a different value of T_{2s}. The above equation yields the well-known dependence with the surface to volume ratio (*Sp/Vp)* of a single (closed) pore (Figure 1). The strength of interactions with the solid is usually expressed as the surface relaxivity ρ_2 or relaxation velocity at the pore surface defined as $\rho_2 = \varepsilon_S / T_{2S}$. Using typical values of surface relaxivities between 1 and 10 μm/s, the relaxation time of water located in a sheet-like pore of thickness 1 nm for example (hence V/S=1nm) will be in the range 0.1 to 1 ms. Such values are easily accessible to most commercial spectrometers and to some in-situ logging instruments. Therefore, NMR has the capability for detecting and quantifying the mass of water present in very small pores. However, there are two important issues. First, in nanopores, the measured relaxation time may not give an indication of the pore size (or thickness for a sheet) according to equation 1 because the length scale of the NMR interactions are comparable to the thickness (a few nanometer compared to ε_S~0.5 nm). This is indeed the case in the interlayer space of smectites [1] in which equation 1 has been found not to be valid. Second, the diffusive exchange between pores [5] may lead to a T_2 distribution that does not represent anymore a pore size distribution, and hence the classical method for deducing capillary bound water using a cut-off is not applicable. Indeed, taking a typical macroscopic water effective diffusivity of 1 10^{-10} m^2/s (as shown later), a typical

diffusion length $(6Dt)^{1/2}$ at time t=1ms is 800 nm. This is well above the typical range of pore size usually encountered in shales. We will give experimental proofs of the diffusive coupling in future work.

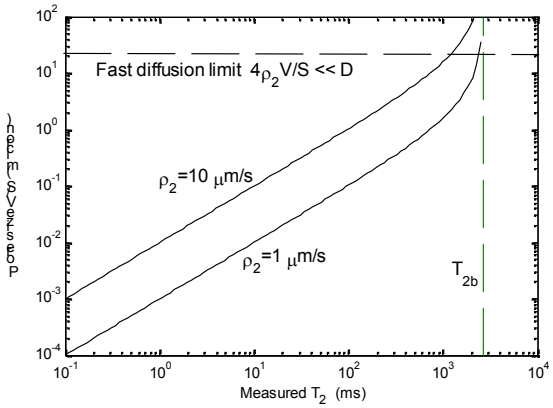

Figure 1: Graphical representation of equation 1 with two surface relaxivities covering the range of usual values.

Relaxation of pseudo-solid material

A consequence of the fast exchange model described above is that the measured relaxation time cannot be smaller than T_{2S}. Very short relaxation times (<0.1 ms or less than T_{2S}) are produced by processes related to the mobility of protons. The theoretical framework is the so-called Bloembergen-Purcell-Pound (BPP) model relating the longitudinal and transverse relaxation times to the correlation time τ of the dipolar interaction:

$$\frac{1}{T_1} = 2C\left[\frac{2\tau}{1+\omega^2\tau^2} + \frac{8\tau}{1+4\omega^2\tau^2}\right] \qquad (2)$$

$$\frac{1}{T_2} = C\left[6\tau + \frac{10\tau}{1+\omega^2\tau^2} + \frac{4\tau}{1+4\omega^2\tau^2}\right]$$

where ω is the Larmor frequency and C is a constant. A single value of correlation time is assumed here for simplicity. For fast isotropic molecular tumbling, as is the case in the above mentioned fast diffusion model, $\omega\tau << 1$ and $T_1/T_2=1$ (in fact, due to the heteronuclear dipole-dipole interactions with the electronic spins, we have $T_1/T_2\sim2$). When molecules are not mobile, the correlation time is several orders of magnitude larger, $\omega\tau >> 1$, and the ratio $T_1/T_2\sim\omega^2\tau^2$ is much larger than 1 and depends on the Larmor frequency. For example for ice, T_1=70 s and T_2=8 μs at 30 MHz. A large T_1/T_2 ratio is seen in many materials of interest for the petroleum industry: heavy oil, coal, organic matter.

Relaxation of methane

For bulk methane in the gas phase (i.e. at temperature of interest here), the longitudinal and transverse relaxation mechanisms are dominated by spin rotation [6], in contrast with intra and intermolecular interaction occurring in simple liquids (or in liquid methane). T_1

and T_2 are still equal and governed by equation 2, but they increase with pressure and are in the range [500-5000 ms] for methane pressure between 25 up to 200 bar. More interestingly in rock core materials [7] or for adsorbed gas in nanoporous material [8] at low temperature (100K), the T_1/T_2 ratio of methane increases considerably (~10 or more). This is due to anisotropic rotational motions at the surface, with the existence of two correlation times. T_1 will then be sensitive to the fast correlation time, while T_2 to the slow one. In a partially saturated porous media, relaxation of methane still occurs although weaker despite water wetting the surface [7].

MATERIALS AND NMR METHODS

NMR methods

The experiments have been carried out on a Maran Ultra proton spectrometer from Oxford Instruments with a proton Larmor frequency of 23.7 MHz. Standard free induction decay (FID) and transverse magnetization CPMG decay curves were measured. When needed, we used a modified CPMG sequence in which the inter-echo time is initially set at the lowest possible and then increased gradually up to 100 μs or more in order to catch at the same time very short and very long relaxation times. 2D T_1-T_2 maps were determined using an inversion recovery sequence followed by a CPMG sequence:

$$P_{180} - \tau_1 - P_{90} - (\tau - P_{180} - \text{echo-})_n$$

where τ_1 takes usually 40 discrete values spaced logarithmically, and the number of echo n is adjusted in order to reach zero signal (noise level). Hence, we obtain a magnetization function of two times, τ_1 and $n\tau$, later analyzed in terms of a T_1-T_2 2D map computed with an in-house 2D inverse Laplace transform software.

Table 1: Main characteristics of the NMR instrument. P90 is the 90° pulse duration.

Probe diameter (mm)	Probe dead time (μs)	P90 (μs)	Filter dead time 100kHz/1MHz (μs)	τ spacing (μs)	1st FID (μs)
10	5	2	15	25	21
			5	15	11
18	15	6	15	30	33

We used two NMR probes of diameter 10 and 18 mm depending on the desired information and size of samples. The capacity of detecting "solid like protons" with very short relaxation times depends critically on the probe dead time. Using a small probe diameter of 10 mm reduces significantly the dead time down to 5 μs compared to the standard 18 mm probe (Table 1). It also reduces the 90° pulse duration to insure a larger frequency bandwidth when detecting solid protons. In addition, the filter dead time can be reduced significantly using a 1 MHz bandwidth, at the expenses however of the signal to noise ratio. Note that the smallest τ spacing available is 15 μs and hence, the first acquired point in the CPMG decay is at 30 μs.

For diffusion measurements, we used a deuterium exchange technique described in detail elsewhere [9]. For water saturated samples, it allows the determination of tortuosity and the detection of non-connected porosity, if any.

The high pressure NMR cell is custom-build and entirely made of non-magnetic and non-conducting material (PEEK). Such material gives a NMR signal at around 0.08 ms and is therefore not suited for detecting this range of relaxation times, corresponding mostly to hydroxyls in clay rich rock samples. It was designed for the 18 mm probe, the maximum sample size is 8 mm in diameter and 20 mm in length (Figure 2). It can sustain up to 200 bar at 30 °C and it has been tested up to 541 bar, at which pressure it will leak (but not break). The cell is connected to a 500 cc single cylinder pump to vary the pressure from 20 up to 200 bar. With low porosity samples such as shales, dead volumes around the samples can represent 90 % of the signal. Hence, a fine sand was introduced around the sample and in the tube above to reduce these dead volumes.

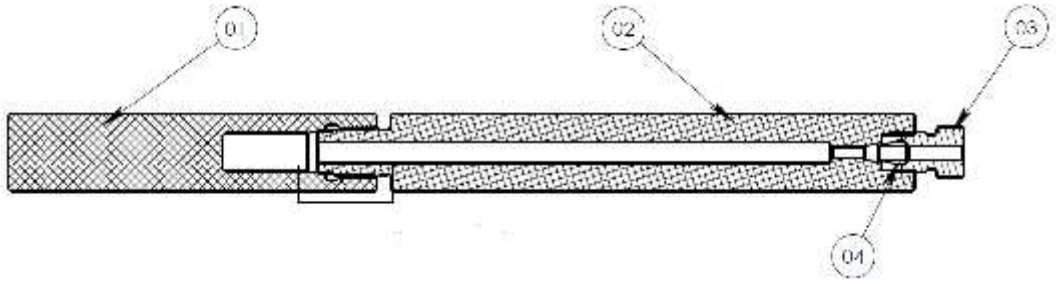

Figure 2: High pressure NMR cell (200 bar). The sample can be placed in the compartment at the left (in part 1, dia. 8mm, length 20mm).

Samples

We used various samples from various origins in order to test the NMR responses of pseudo-dry materials and in the presence of methane. Core samples and organic matter samples extracted from core samples were used and are described in details elsewhere [10]. Three samples of different maturity were available (see figure 9 in Romero-Sarmiento et al. 2014): from a gas (Blakely) and an oil zone (Mesquite), and immature (outcrop).

The results on another shale sample (labelled RM9, Horn River) are also presented. The sample originates from a gas zone and has a total organic content of about 7%. No particular cleaning was performed. To ensure full water saturation, the sample was kept under high static pressure during several days. To dry the sample, a standard protocol was applied (oven dry at 60°C until a stable mass is reached). Since no particular care was taken to keep the sample in dry air, this is only a pseudo dry state since water vapour can adsorb in the smallest pores, in equilibrium with the ambient humidity at laboratory temperature, a well-known effect. This is further discussed below. NMR porosity is 7.1% and gas permeability is 2 nD in the dry state, using a steady state technique. For this sample, high pressure mercury injection (HPMI) performed on a nearby sample reveal

very small pore entry sizes (Figure 4). Clearly, in this case, the limit of resolution is reached and HPMI experiments are able to explore only half of the porosity compared to NMR.

Despite the very small pore size distribution, the deuterium exchange experiment reveal a very good connectivity of the pore network. The curve shown in Figure 4 represents the average concentration of water (w.r.t. deuterium) as a function of time while deuterium is diffusing inside the core and water outside. Unconnected porosity would show up as a residual signal at the end of the experiment, but this was not observed. Experimental data can be matched very well with a homogeneous diffusion model. We find an effective diffusion coefficient D_{eff}=0.62 10^{-6} cm^2/s. Defining a tortuosity τ as D_m/D_{eff} (the diffusion coefficient of free water D_m=2.60 10^{-5} cm^2/s at 30°C), we obtain τ= 41.8. The diffusion coefficients can also be compared to a standard Archie relationship according to:

$$\frac{D_{eff}}{D_m} = \Phi^{m-1} \qquad (3)$$

where m is the Archie's cementation exponent. We obtain m=2.45.

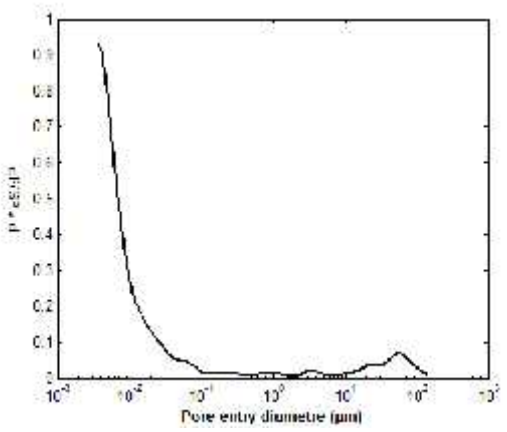

Figure 3: Pore entry size distribution from mercury injection experiments representing reservoir sample RM9. The limit of resolution is reached.

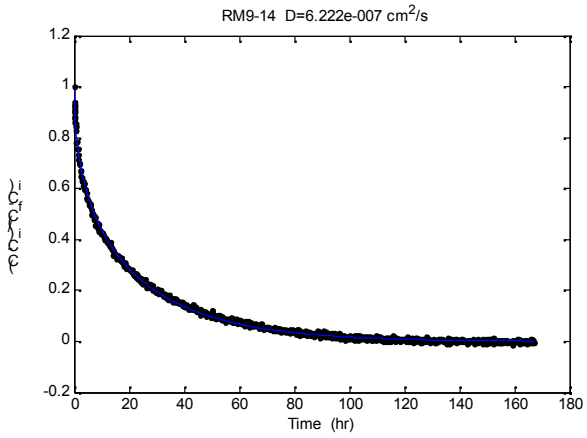

Figure 4: Deuterium diffusion experiment for reservoir sample RM9 (d=15mm, L=15 mm) performed at 30°C . Data (dots) and fit (line).

RESULTS

The instrument used for this study is able to detect all protons present in the samples. For pseudo-dry samples (i.e. samples at equilibrium with the ambient humidity), we are able to detect hydroxyls part of the clay structure and protons from the organic matter. For water or methane saturated samples, the signal will be dominated by water or methane signals and it may be difficult to detect at the same time weak signal originating from

organic matter. Hence, in order to evidence the signature of each element, we studied separately the samples in dry or saturated conditions: dry organic matter (OM) alone, dry samples with the same organic matter, organic matter saturated with methane, dry shale sample, water and methane saturated shale sample.

Organic matter

The signal from dry organic matter extracted from core samples is shown in Figure 5. T_2 values are around 0.1 ms and below in the gas window. When the organic matter is immature, the T_1/T_2 tends to be smaller (~50) than in the oil and gas windows ($180 < T_1/T_2 < 250$). This observation is consistent with the fact that the mobility of protons is expected to be larger for immature organic matter. From FID data and in a similar way as for smectites [1], we can also estimate the total amount of hydrogen present in the samples: from immature, oil and gas OM, we obtain respectively 59 mg/g, 30 mg/g and 21 mg/g of hydrogen per gram of dry material. This is in agreement with the general trend that hydrogen content decreases with maturity. However, no detailed relationship with hydrogen content from standard Rock-Eval analysis could be established.

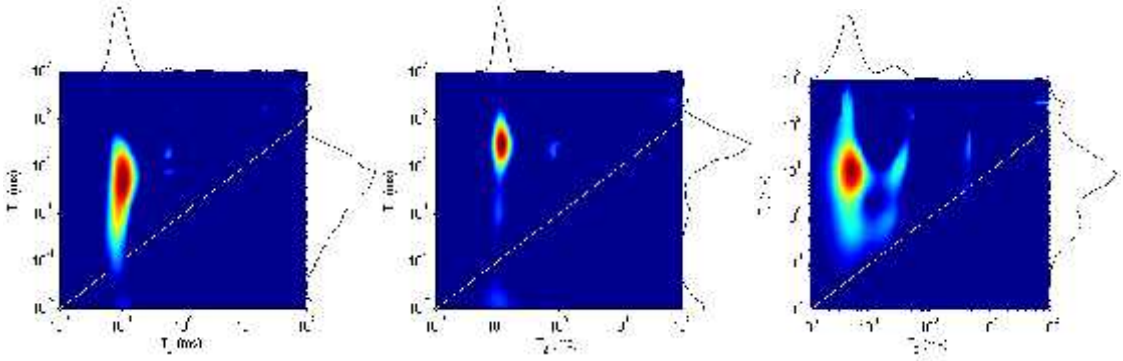

Figure 5: T_1-T_2 maps on three types of organic matter extracted from shale samples. For left to right: immature (T_1/T_2~50), oil (T_1/T_2~250) and gas (T_1/T_2~180) window.

Analyzing now the core samples from which the organic matter was extracted (only two of them were available, Figure 6), we first observe a large signal in the range $0.01 < T_2 < 0.1$ ms, at the limit of T_2 resolution. It is also spread over a wide T_1 range (and easily resolved) and this is typical of hydroxyls from the clay structure. In the oil window, organic matter appears as a secondary peak located at T_2~0.5 ms and T_1~100 ms, in relative agreement with its location when extracted from the samples (T_2~0.1 ms and T_1~50 ms). In the gas window, the OM signal cannot be identified because it overlaps with the hydroxyl signal.

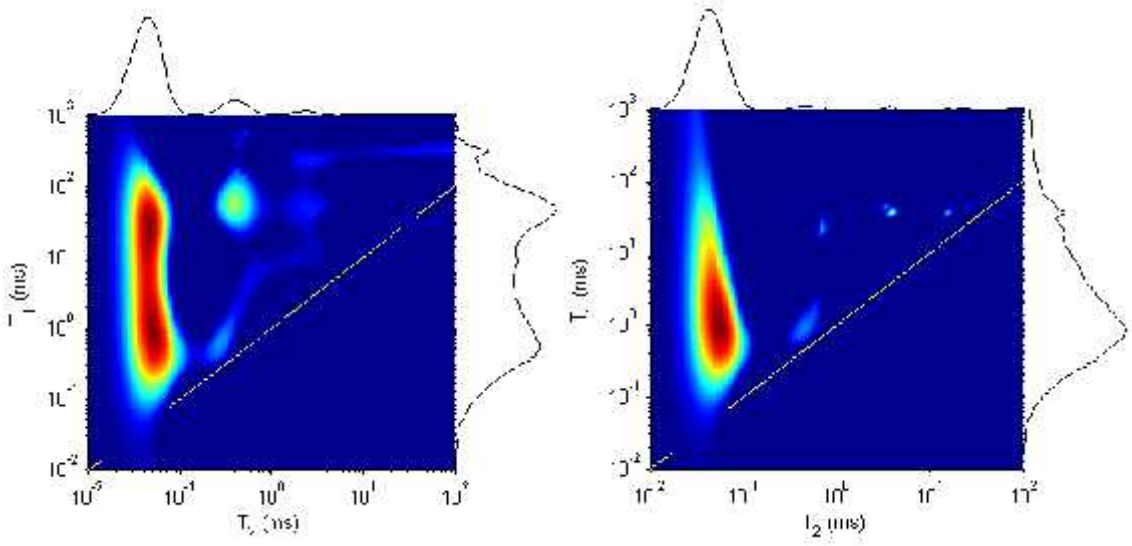

Figure 6: T_1-T_2 maps on two dry shale samples from which organic matter was extracted. Left: oil window; right: gas window. In the gas window, organic matter cannot be distinguished.

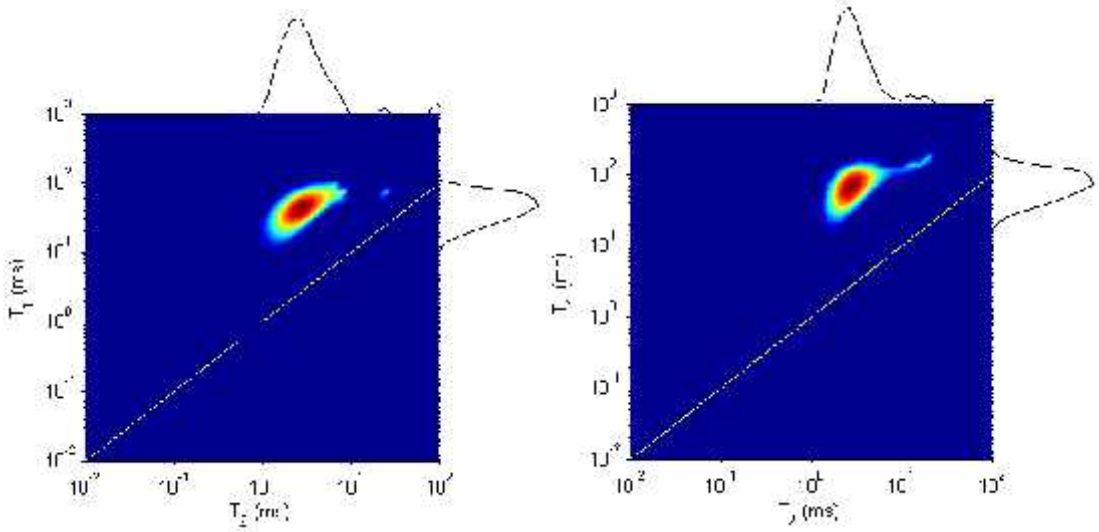

Figure 7: Methane saturated organic matter in the gas window. Left: 100 bar (T_1/T_2~15); right: 200 bar (T_1/T_2~20).

Finally, we also identified the signal of methane saturated organic matter (Figure 7). Because organic matter is a powder and no more compacted in the sample, the signature identified here includes inter and intra-granular porosity. Contrary to water saturated situations, the diffusivity of methane is such that there is an exchange between inter and intra granular pores and therefore, the two porosity compartments cannot be distinguished. The relaxation time T_2 should then be interpreted as proportional to the total volume divided by the total surface; the surface is driven by the internal surface

inside the grains but the volume is driven by the inter-granular porosity. Hence, we expect that the true signature of methane in organic matter in the sample be shifted to lower T_2 values due to smaller volumes in the absence of inter-granular porosity. The T_1/T_2 ratio (between 15 and 20 depending on pressure) is typical of gas interactions with a solid, as will be seen also later.

Shale samples

The RM9 shale sample was also analyzed at different saturation states: dry, water and methane saturated. For the dry sample, the T_1-T_2 map is dominated by the hydroxyl signal with T_2 less than 0.1 ms (Figure 8) and a wide range of T_1 values. Between 0.1 and 1ms, there is some residual water, mainly distinguishable in the T_2 distribution. When saturated with water, we can clearly distinguish the water signal with T_1/T_2~2. To calculate porosity, we took only this signal into account. The water T_2 distribution has essentially two modes, due to an heterogeneity clearly visible in micro-tomography images (not shown, a thin layer of with a high organic matter content in the longitudinal direction). For the methane saturated case (Figure 9), the situation is very different and we have a large contrast between T_1 and T_2, as already expected and observed in organic matter. For this experiment, the large peak (T_2~60 ms and T_1~1000 ms) represents methane in the sand around the sample, and the small peak (T_2~10 ms and T_1~1000 ms) methane in the shale sample. Indeed, even though the shale total volume is dominant, its small porosity (7%) is such that the pore volume in the sand around and at the top of the sample is dominant.

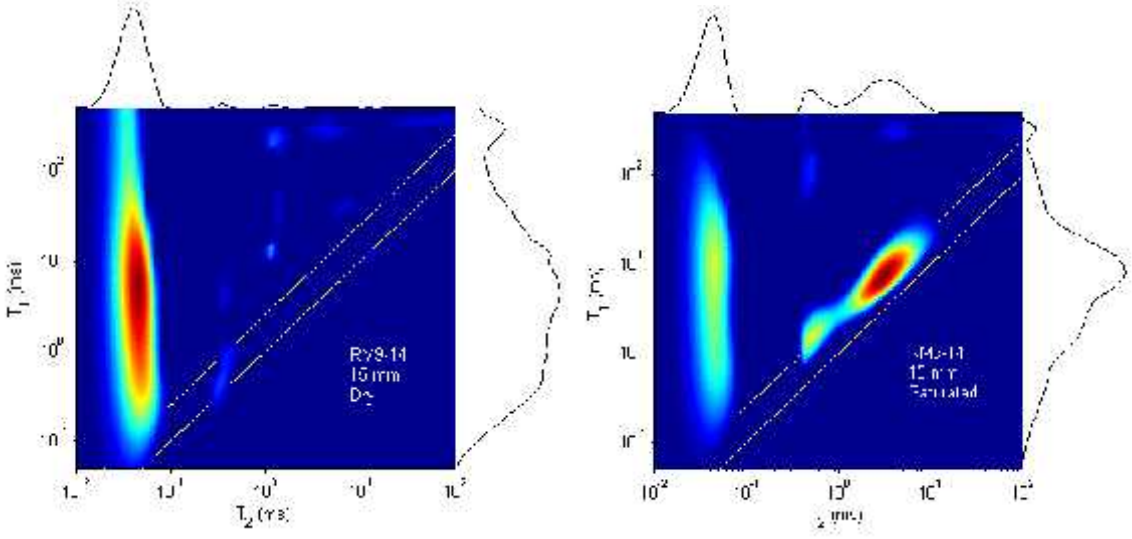

Figure 8: T_1-T_2 maps on 15 mm diameter miniplugs in the dry and water saturated state. The short T_2 signal with a large range of T_1 represents hydroxyls and organic matter. The two lines indicate T_1/T_2=1 and T_1/T_2=2.

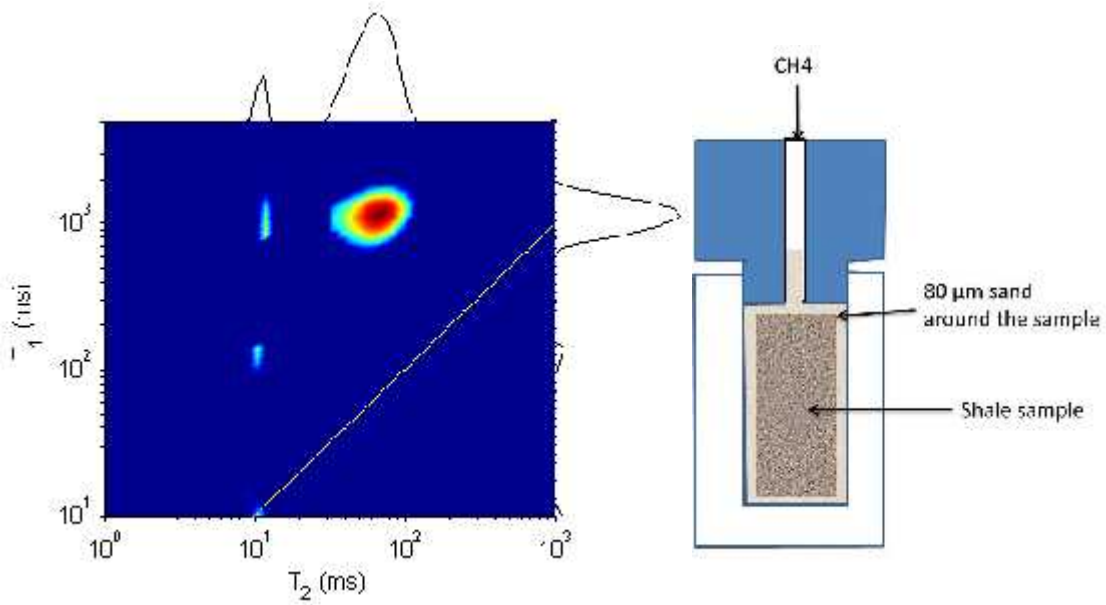

Figure 9: T_1-T_2 maps for methane at 200 bar for sample RM9 (small peak at T_2=10 ms and T_1=1000 ms). The large peak corresponds to the 80 um quartz sand around the sample.

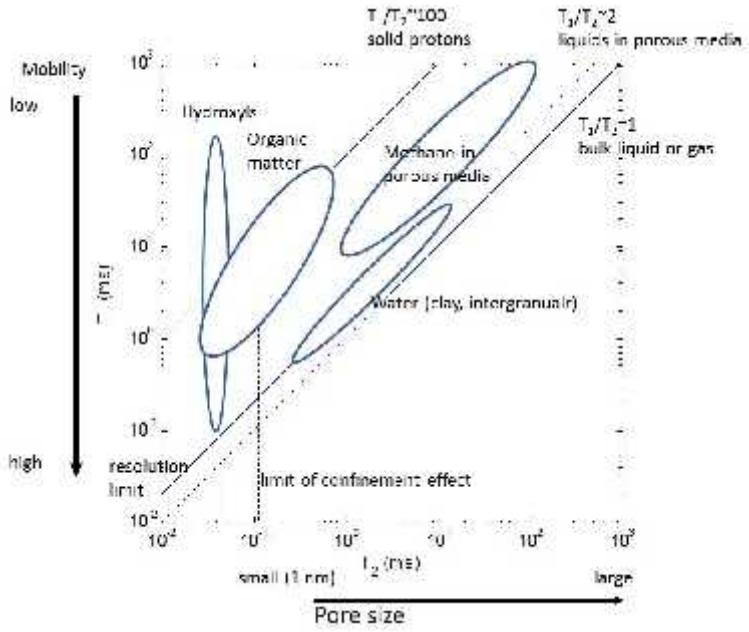

Figure 10: Fluid or proton typing using T_1-T_2 maps

Synthesis : T_1-T_2 fluid mapping

For shale samples, we see that the T_1-T_2 map is a very efficient way to separate the contributions from the different compartments containing hydrogen molecules. The sketch in Figure 10 summarize the results obtained in this study. The T_2 axis represents a pore size after scaling with the surface relaxivity. For a given sample, the distribution of relaxation times may not represent a distribution of pore sizes due to diffusive exchange already mentioned; but if two samples have a different average pore size, the average relaxation time T_2 for these two samples will be different. We have two limits on the T_2 axis: (i) the lowest value that can be reached when water interact with the surface (relaxation time T_{2S} of water molecules that would be permanently at the solid surface) and (ii) the resolution limit linked to the instrument used; it can be evaluated by taking the inter-echo time; for example in our case and depending on the probe 0.06 ms. The T_1 axis represents roughly the proton rotational mobility: for large T_1/T_2 ratio, the mobility is small; for solid protons, it also corresponds to reduced molecular mobility.

The different protons in the T_1-T_2 map can be associated with the following origins:

- Hydroxyls: OH part of the clay structure or at the edges of clay platelets; this signal is always at the limit of resolution, below 0.1 ms. It can only be detected with appropriate NMR instruments,
- Protons part of the organic matter: depending on the maturity, they can overlap with hydroxyls. They can be best detected in dry samples since their hydrogen index is quite low compared to water,
- Water: this signal is typically located on or close to the line T_1/T_2~2 even for very small pore sizes such as interlayer space in clays,
- Methane: when considering T_2 only, this signal can overlap with the water signal, as noted by other authors [11]. However when considering T_1, it can easily be separated because T_1/T_2~10. Such ratio is consistent with other measurements [7] and depend slightly on pressure. Adsorbed methane has no specific signature because it is in fast exchange with free methane.

We did not consider yet the signature of oil. With light oil, we expect a ratio close to 2. For heavy oil or bitumen, it may increase largely [3].

CONCLUSION

We evidenced the signature of the 4 protons populations present in shale samples in a T_1-T_2 map: hydroxyls from the clay structure, protons from the organic matter, water and methane at various pressure. These signatures have been determined on organic matter alone, and shale samples at different saturation states. In a T_1-T_2 map, these signatures do not overlap, except for organic matter with high maturity. The position of these signatures is qualitatively well understood from NMR relaxation theory as well as existing work on methane in porous media.

AKNOWLEDGEMENT

We thank Maria Romero-Sarmiento for providing the organic matter samples, and ExxonMobil Upstream Research Co. for allowing us to use some results of an unpublished study.

REFERENCES

[1] Fleury M, Kohler E, Norrant F, Gautier S, M'Hamdi J, Barré L. Characterization and Quantification of Water in Smectites with Low-Field NMR. J. Phys. Chem. C 2013;117:4551–60.

[2] Washburn KE, Birdwell JE. Updated methodology for nuclear magnetic resonance characterization of shales. J. Magn. Reson. 2013;233:17–28.

[3] Rylander E, Singer PM, Jiang T, Lewis R, Mclin R, Sinclair S. NMR T 2 Distributions in the Eagle Ford Shale : Reflections on Pore Size. SPE 164554, 2013.

[4] Kausik R, Minh C, Zielinski L. Characterization of Gas Dynamics in Kerogen Nanopores by NMR. SPE 147198, 2011, p. 1–16.

[5] Fleury M, Soualem J. Quantitative analysis of diffusional pore coupling from T2-store-T2 NMR experiments. J. Colloid Interface Sci. 2009;336:250–9.

[6] Oosting PH, Trappeniers NJ. Proton-Spin-Lattice Relaxation and Self-diffusion in methanes III. Interpretation of proton-spin-lattice relaxation experiments. Physica 1971;51:395–417.

[7] Straley C. An experimental investigation of methane in rock materials. SPWLA 38th Annu. Logging Symp., 1997.

[8] Riehl JW. NMR Relaxation of Adsorbed Gases: Methane on Graphite. J. Chem. Phys. 1972;57:2199.

[9] Berne P, Bachaud P, Fleury M. Diffusion Properties of Carbonated Caprocks from the Paris Basin. Oil Gas Sci. Technol – Rev. l'Institut Français Du Pétrole 2009;65:473–84.

[10] Romero-Sarmiento M-F, Rouzaud J-N, Bernard S, Deldicque D, Thomas M, Littke R. Evolution of Barnett Shale organic carbon structure and nanostructure with increasing maturation. Org. Geochem. 2014;71:7–16.

[11] Tinni A, Odusina E, Hughes B, Sulucarnain I, Sondergeld C, Rai C. NMR Response of Brine , Oil , and Methane in Organic Rich Shales. SPE 168971, 2014.